OATAO
Open Archive Toulouse Archive Ouverte

Open Archive TOULOUSE Archive Ouverte (OATAO)

OATAO is an open access repository that collects the work of Toulouse researchers and makes it freely available over the web where possible.

Any correspondance concerning this service should be sent to the repository administrator: staff-oatao@listes-diff.inp-toulouse.fr

Electrical behaviour of a silicone elastomer under simulated space environment

A Roggero[1,2], E Dantras[1], T Paulmier[2], C Tonon[3], N Balcon[4], V Rejsek-Riba[2], S Dagras[3] and D Payan[4]

[1] Physique des Polymères, Institut Carnot CIRIMAT, Université Paul Sabatier, 108 route de Narbonne, 31062 Toulouse Cedex 04, France
[2] ONERA, The French Aerospace Lab F-31055, France
[3] Airbus Defence and Space, 31 Avenue des Cosmonautes, Toulouse 31402, France
[4] Centre National d'Etudes Spatiales, 18 Avenue Edouard Belin, Toulouse 31400, France

E-mail: eric.dantras@univ-tlse3.fr

Abstract

The electrical behavior of a space-used silicone elastomer was characterized using surface potential decay and dynamic dielectric spectroscopy techniques. In both cases, the dielectric manifestation of the glass transition (dipole orientation) and a charge transport phenomenon were observed. An unexpected linear increase of the surface potential with temperature was observed around T_g in thermally-stimulated potential decay experiments, due to molecular mobility limiting dipolar orientation in one hand, and 3D thermal expansion reducing the materials capacitance in the other hand. At higher temperatures, the charge transport process, believed to be thermally activated electron hopping with an activation energy of about $0.4\,eV$, was studied with and without the silica and iron oxide fillers present in the commercial material. These fillers were found to play a preponderant role in the low-frequency electrical conductivity of this silicone elastomer, probably through a Maxwell–Wagner–Sillars relaxation phenomenon.

Keywords: silicone, electrical conductivity, potential decay

(Some figures may appear in colour only in the online journal)

1. Introduction

Room temperature vulcanization (RTV) silicone elastomers are being used extensively in the aerospace industry [1], mainly as adhesives (solar cells, cover glasses, electrical wires) and sealants. These materials are usually filled with inorganic particles to enhance their mechanical (increased tear resistance, reduced thermal expansion in bonded assemblies) [2, 3], thermal [4] or electrical (surface charge dissipation) [5] properties, or facilitate their implementation (increased viscosity, dyeing). While the mechanical improvements brought to silicone rubbers by the inclusion of silica fillers is well documented, and in spite of the wide use of these composite materials in the field of electrical insulation, their electrical behavior has received relatively low attention [6–9].

In aerospace applications, one of the main concerns is electrostatic discharges (ESD) which are caused by low-energy electrons depositing at the surface of the satellite thus building up high potentials on insulating materials [10]. Proper understanding of the electrical behavior and its temperature dependence is therefore essential to anticipate the ability of a material to dissipate surface charge.

For that purpose, surface potential decay (SPD) measurements have been widely employed since the sixties. This technique consists in charge deposition through an electron beam in vacuum [11, 12] or, most frequently, a corona discharge in air [13–15]. Surface potential kinetics can be monitored with a potential probe as a function of time, with a possible temperature ramp rate. Possible physical phenomena accounting for such a potential decay are charge injection (only with corona discharge), surface conduction and charge neutralization, bulk conduction, or dipolar polarization [16].

While SPD has been widely employed to characterize the electrical conduction of insulating materials, molecular

mobility and associated dipolar relaxation studies have generally been limited to dynamic dielectric spectroscopy (DDS) [17] (isothermal ac measurements) and thermally stimulated currents (TSC) analysis [18] (thermally stimulated dc depolarization currents measurements).

With this study, we present a new experimental approach, named Thermally Stimulated SPD (TSSPD), that allows the observation of both dipolar relaxations and charge transport in polymers. Moreover, there are similarities between this technique and the environment coating materials are exposed to in space applications (vacuum, low-energy electrons, low temperature and large thermal steps). TSSPD was performed on rare occasions in the past [19, 20], but with the use of corona discharge (instead of an electron beam) at high-temperature followed by the sample cooling down (instead of low-temperature charging and sample heating up). We will highlight two noteworthy phenomena occurring during such experiment, and assumptions will be formulated about their physical origin.

2. Materials and methods

2.1. Material

This study focuses on a commercial (Wacker) bi-component silicone elastomer which reticulates at room temperature. Part A mainly consists of a polyphenylmethylsiloxane resin (approx. 35 wt%) mixed with crystalline silica (α-quartz particles of the glass splinters type, the size of which is comprised in the range [0.2;20 μm]) and iron(III) oxide (Fe_2O_3 particles the size of which is comprised in the range [0.1;1 μm], with an aspect ratio of 1) fillers. Part B is a hardener containing a Pt catalyst responsible for the polymerization. The two components are manually mixed (weight ratio 9:1) and poured into a mold consisting in a 50×50 mm^2 aluminum substrate the borders of which had been covered with aluminum tape. Despite its ability to reticulate at room temperature, a curing process of 6 h at 100 °C was chosen to enhance the sample reproducibility.

A filtration process performed on part A, allowed the removal of the vast majority of the fillers from it. Consecutive polymerization with unmodified part B led to the formation of *neat* samples (no fillers), as opposed to *filled* standard samples (with fillers).

2.2. Differential scanning calorimetry

Differential scanning calorimetry (DSC) measurement was performed in a TA Instruments apparatus under helium. The sample (mass 9.4 mg) was analyzed in a sealed aluminum pan, at a heating rate of + 20 °C min^{-1}.

2.3. Dynamic mechanical analysis

The dynamic mechanical analysis (DMA) was performed under nitrogen on a Rheometrics Scientific ARES G2 manufactured by TA Instruments. 300 μm -thick adhesive film was analyzed in parallel plates mode, over the linear elastic range. Torque measurements at constant strain ($\gamma = 0.1\%$) and

constant angular frequency ($\omega = 1$ rad.s^{-1}) lead to the complex shear modulus G^* (ωT):

$$G^*(\omega, T) = G'(\omega, T) + iG''(\omega, T) \tag{1}$$

where G' and G'' are the conservative and dissipative moduli, respectively.

The dissipation factor $\tan(\delta)$ is the ratio of the dissipative and conservative moduli.

2.4. Surface potential decay

Surface potential decay (SPD) experiments were performed in the MARCEL facility at ONERA. Under high vacuum (10^{-7} mbar), 170 μm-thick film samples were irradiated under a 10 KeV electron beam in order to build surface charge. Surface potential relaxation was then monitored through the use of a vibrating Kelvin probe. The sample holder was thermally regulated by liquid nitrogen and a heating resistor. Temperatures as low as -180 °C could be reached. During TSSPD experiments, the electrical charge was deposited at low temperature (-150 °C) and a temperature ramp of $+5$ °C min^{-1} was subsequently set up during the potential decay step.

2.5. Dynamic dielectric spectroscopy

Broadband dielectric spectroscopy measurements were performed isothermally (5 °C steps between -150 and $+100$ °C), in the frequency range of 10^{-2} to 10^6 Hz, using a Novocontrol impedance analyzer BDS 4000. 170 μm-thick adhesive films were placed between gold-plated stainless steel electrodes ($\varnothing = 30$ mm).

Complex permittivity (equation (2)) and conductivity (equation (3)) were calculated based on experimental values of impedance.

$$\varepsilon^*(\omega) = \varepsilon'(\omega) - i\varepsilon''(\omega) = \frac{1}{i\omega C_0 Z^*(\omega)} \tag{2}$$

$$\sigma^*(\omega) = \sigma'(\omega) + i\sigma''(\omega) = i\omega\varepsilon_0\varepsilon^*(\omega) \tag{3}$$

3. Results and discussion

3.1. Physical structure

DSC scans revealed the value of the glass transition temperature T_g of the filled material: -116 °C, which is in good agreement with literature [21–23]. By means of DMA, its viscoelastic transition temperature T_α was found to be -117 °C, very close to T_g. As seen in figure 1, these two techniques are in very good agreement.

It should be noted that absolute values of moduli are not reliable in the glassy region as the materials becomes too rigid for the chosen experimental configuration.

3.2. Isothermal dielectric behavior

The isothermal dielectric behavior of the filled material was characterized by means of DDS.
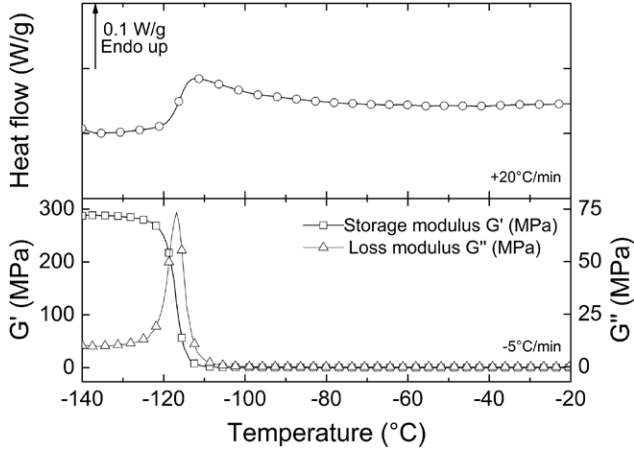
Figure 1. DSC (up) and DMA (down) thermoanalytical curves.

The 3D dielectric loss spectrum represented in figure 2 features one dipole relaxation mode, called α, associated with the dielectric manifestation of the glass transition. From each isothermal curve comprising the α-mode, the Havriliak–Negami [24] parametric equation (equation (4)) was used to extract a mean dipole relaxation time $\tau_{H-N}(T)$.

$$\varepsilon^* = \varepsilon_\infty + \frac{\varepsilon_s - \varepsilon_\infty}{(1 + (i\omega\tau_{H-N})^{\alpha_{H-N}})^{\beta_{H-N}}} \qquad (4)$$

where ε_∞ and ε_s are respectively the high and low frequency limits of the real part of complex permittivity, ω the angular frequency, and α_{H-N} and β_{H-N} the Havriliak–Negami adjustable parameters. All of the fitted relaxation times are displayed in the Arrhenius plot in figure 3.

The α-mode unsurprisingly [17] obeys the Vogel–Fulcher–Tamman (VFT) law (equation (5)).

$$\tau(T) = \tau_0 e^{\frac{1}{\alpha_f(T-T_\infty)}} \qquad (5)$$

where τ_0 is a pre-exponential factor, T_∞ the ideal glass temperature below which there is no free volume and α_f the coefficient of thermal expansion of free volume above T_∞. The VFT fit parameters of the α-mode are listed in table 1.

The ideal glass transition temperature T_∞ is located 23 °C below the calorimetric T_g temperature:

$$T_\infty \approx T_g - 23 \ ^\circ C \qquad (6)$$

At higher temperatures, a conductivity rise was observed. A sub-T_g dipolar mode, marked MWS in figure 2, seems to be superimposed to the conductivity contribution. It is probably due to the polarization of macrodipoles at the fillers/polymer interface called Maxwell–Wagner–Sillars polarization [25]. It is the scope of part 3.3.2. of this study.

3.3. Thermally stimulated dielectric behavior

The TSSPD technique was used on a 170 μm-thick filled silicone film (figure 4). Following the charging step performed at $T = -150\,°C$ ($V_0 \approx -4$ kV), a +5 °C min^{-1} temperature ramp rate was then applied to the sample, up to room temperature, during the potential decay step.
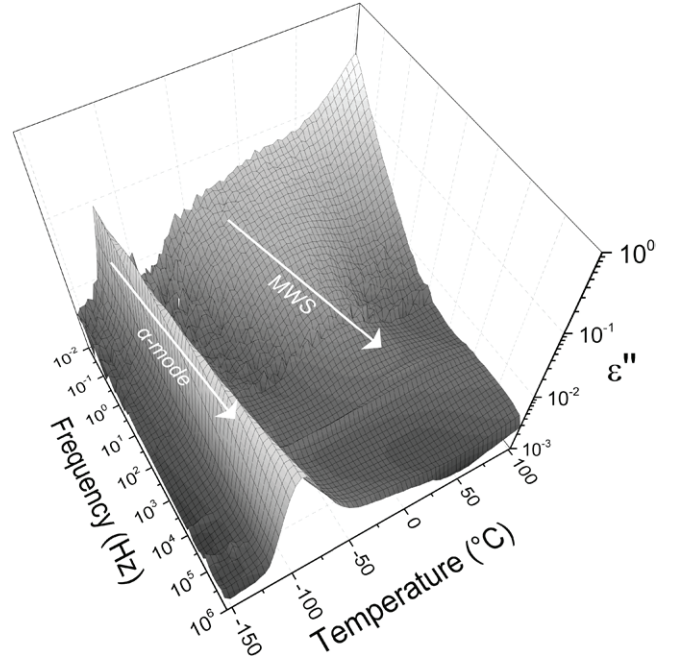

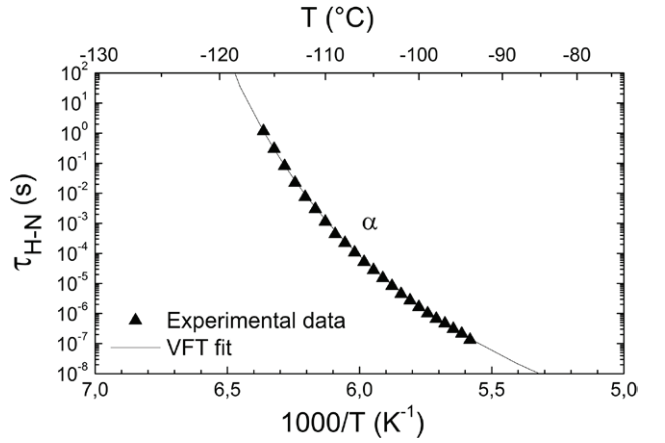**Figure 2.** DDS 3D spectrum of dielectric loss versus frequency and temperature.

Figure 3. Arrhenius plot of the Havriliak–Negami relaxation times and VFT fit (extrapolated to higher and lower temperatures).

Table 1. VFT fit parameters of the α-mode.

τ_0 (10^{-15} s)	3
α_f (10^{-3} K^{-1})	1.3
T_∞ (K)	134
T_∞ (°C)	~ −139

Two distinct phenomena are noticeable on figure 4 and are arbitrarily associated with two regions:

- Region I: in the range [−125, −110 °C], a 14% surface potential drop appears as the sample is heated above the glass transition temperature of the material.
- Region II: above approximately −50 °C, a continuous decrease of surface potential until quasi-complete discharge of the sample is observed.
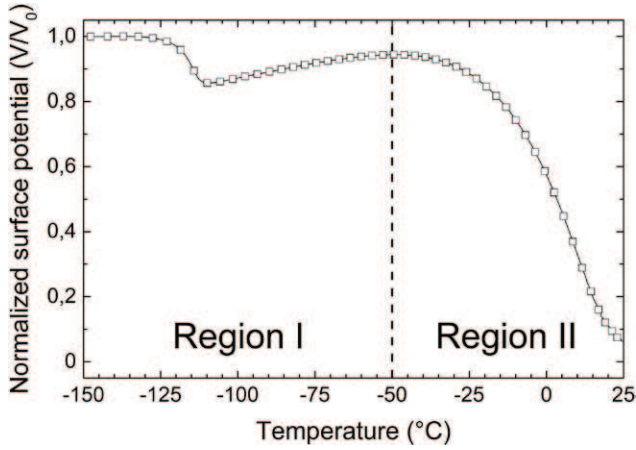
Figure 4. TSSPD of a 170 μm-thick silicone elastomer film initially charged under 10 keV electron irradiation ($V_0 = -4$ kV).

Figure 5. Consecutive TSSPD around T_g.

3.4. Region I: dipole orientation at glass transition

The potential drop occurring near calorimetric T_g is believed to be the dielectric manifestation of the glass transition i.e. the orientation of main chains dipoles along the electric field induced by the electrical charges initially deposited at the surface. In order to confirm this hypothesis, thermal cycling was performed around T_g and is shown in figure 5. After an initial charge deposition at $T = -150$ °C, three temperature steps ($-150 \rightarrow -70$ °C, $-70 \rightarrow -150$ °C and $-150 \rightarrow +25$ °C) were successively performed without subsequent charge injection.

Unsurprisingly, the first temperature ramp led to the same potential drop as observed in figure 4. The sample was initially cooled down to -150 °C $< T_\infty$, thus freezing α-dipoles in random orientations and preventing them from aligning with the electric field generated by the charging process. During the first ramp, the sample was heated beyond T_g, temperature above which the dipoles obtained sufficient mobility to preferentially align themselves with the external electric field (they are rotated by a few degrees). In this way, a macroscopic polarization was induced, being itself the source of a depolarization field of opposite sign with regard to the initial external electric field, leading then to a decrease of the absolute apparent surface potential.

During the second temperature ramp, the previously observed potential rise was not observed. Assuming dipolar orientation occurred during the first ramp, this observation is coherent because there is no reason why dipoles should relax as temperature is decreased back to -150 °C.

Finally, the third temperature ramp brought the sample from -150 °C (below T_g) up to room temperature. The second and third potential relaxation curves are superimposed, meaning that all available dipoles were initially oriented at the end of the first temperature ramp. If this process presents similarities with the thermally stimulated current analysis (TSC) technique, it is fundamentally different in the fact that dipole orientation (i.e. polarization) is observed in TSSPD while depolarization currents are measured in TSC. In TSC, the sample is macroscopically polarized while the temperature i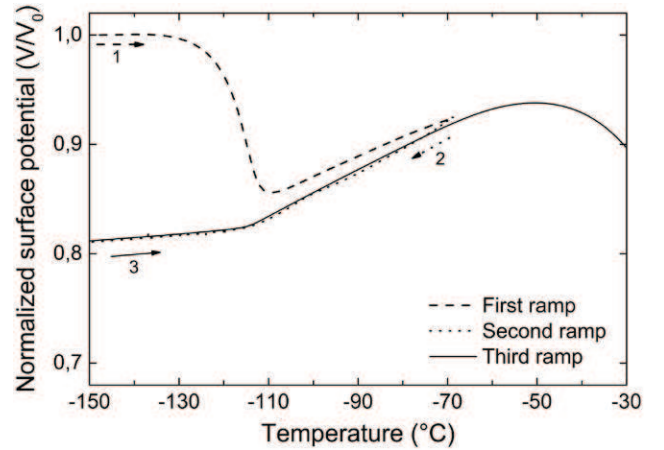s brought from a relatively high temperature (far above T_g) to a low temperature (below T_g), therefore freezing dipole orientation. The macroscopic sample polarization is then removed and a positive temperature ramp is applied, allowing the observation of depolarization currents induced by dipole disorientation.

All of the reasoning above is summarized and exaggerated for clarity reasons in figure 6.

Surface potential relaxation during the second and third temperature ramps also clearly evidence an unexpected linear increase of the surface potential with temperature. The slope dV/dT of this linear dependence takes two distinct values below and above T_g which are reported in table 2. No charge injection was performed subsequently to the initial charging step at $T = -150$ °C, so that the observed potential increase does not traduce any increase of the surface charge. The explanation of this behavior resides in the influence of temperature on both the experimental configuration through thermal expansion of the sample (the experimental linear coefficients of thermal expansion are listed in table 2) and the dielectric properties of the material (through the evolution of its relative permittivity ε').

If one considers, from a rather simplistic point of view, the film sample as a parallel plate capacitor, equations (7) and (8) respectively define its capacitance C(F.m^{-1}) and the potential difference between the two plates U, which is equal to the surface potential V, the second plate being grounded.

$$C = \varepsilon_0 \varepsilon' \frac{A}{l} \tag{7}$$

$$U = \Delta V = V_s = \frac{Q}{C} = \frac{Q}{A\varepsilon_0 \varepsilon'} l \tag{8}$$

where ε_0 (F.m^{-1}) is the vacuum permittivity, A(m^{-2}) the area of the film, l(m) its thickness and Q(C) the deposited electric charge.

Combining equations (7) and (8), and then differentiating the natural logarithm of potential difference leads to equation (9).

$$\frac{dV}{V} = \frac{d\left(\frac{Q}{A}\right)}{Q/A} - \frac{d\varepsilon'}{\varepsilon'} + \frac{dl}{l} \tag{9}$$
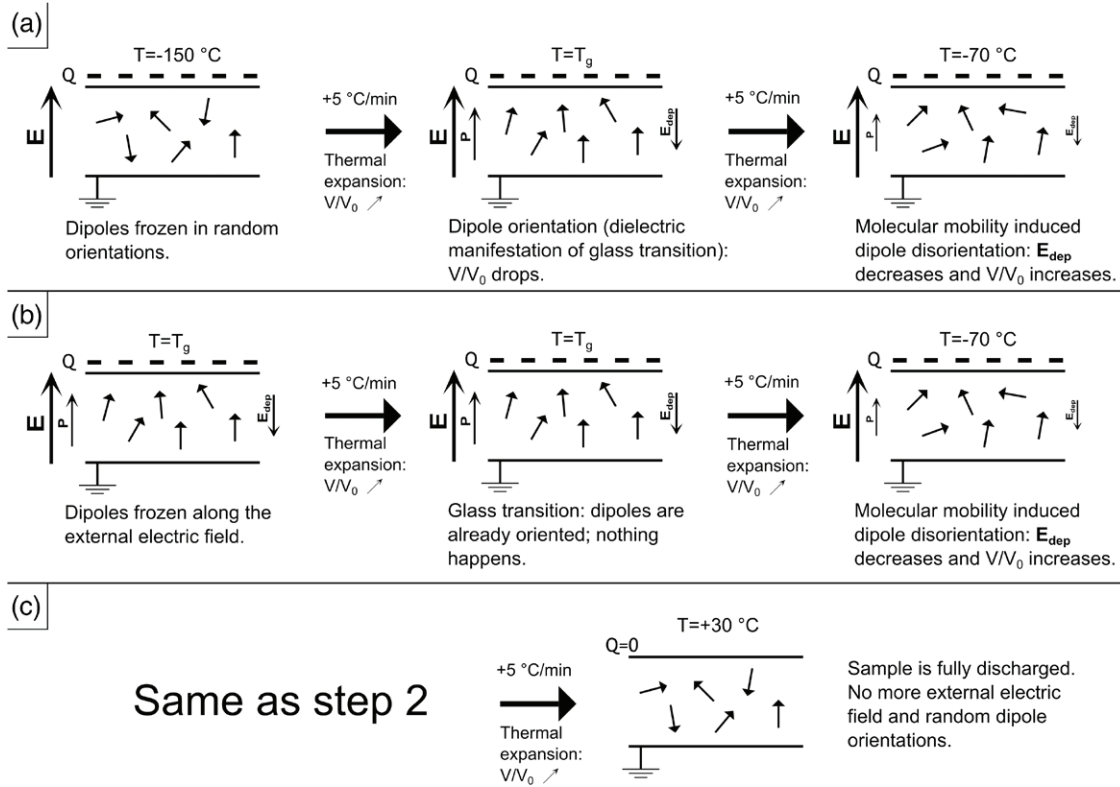
Figure 6. Schematic representation of the physical origins of the experimental curves in figure 5 for (*a*): the first ramp, (*b*): the second ramp, (*c*): the third temperature ramp.

Table 2. Comparison of surface potential relaxation slopes with experimental linear coefficients of thermal expansion, below and above T_g.

	$d(V/V_0)/dT (10^{-6}$ K$^{-1})$	α_l $(10^{-6}$ K$^{-1})$
$T < T_g$	425	70
$T > T_g$	2510	265

As the temperature of the sample is increased, its thickness l and area A expand, but the total surface charge Q initially deposited remains constant in the temperature range investigated (this is evidenced by the superimposition of temperature steps 2 and 3 in figure 5). On the contrary, the experimentally probed area A_p remains constant while the probed charge Q_p evolves as the sample expands or contracts due to temperature variations. The simplest way of dealing with this issue is to take into account the surface charge density $\rho_s = Q/A = Q_p/A_p$ rather than area and charge individually.

The surface potential drop experiment was repeated (figure 7) with different charging times, which resulted in initial surface potentials V_0 in the range $[-300\text{V}; -5\text{kv}]$. For initial potentials greater than about -1 kV, the potential drop observed at T_g seemed to reach a saturation level. Indeed, further increasing the initial potential V_0 (up to -5 kV) did not result in an increase of the potential drop at T_g. This probably means that all contributing dipoles are maximally oriented above this 'saturating field' of roughly 6 MV.m^{-1}. In other words, provided that the saturation condition is maintained, one can assume that the surface charge density has no impact on the thermal evolution of the surface potential: the $d(Q/A)/Q/A$
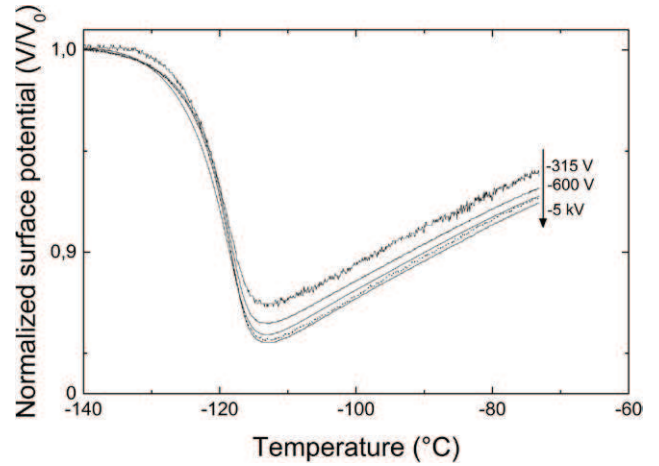

Figure 7. Influence of initial potential on dipole orientation.

contribution might be neglected. Equation (9) is then converted into the following equation:

$$\frac{dV/V}{dT} = -\frac{\frac{d\varepsilon'}{\varepsilon'}}{dT} + \frac{\frac{dl}{l}}{dT} = -\frac{\frac{d\varepsilon'}{\varepsilon'}}{dT} + \alpha_l \quad (10)$$

Where dT is the temperature variation and α_l the coefficient of linear thermal expansion.

If the local electrical field equals the overall applied field, which is a large approximation, then $\varepsilon' - 1 = \alpha N$ where α is the molecular polarizability and N the volume density of molecules, and $d\varepsilon'/\varepsilon'$ is described by equation (11).
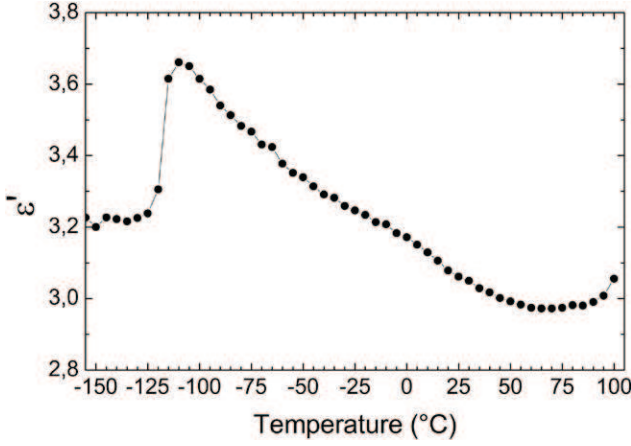
Figure 8. DDS measurements of relative permittivity versus temperature.

Figure 9. Successive isothermal scans over the length of a sample initially charged in its center.

$$\frac{d\varepsilon'}{\varepsilon' - 1} = \frac{d\alpha}{\alpha} + \frac{dN}{N} \qquad (11)$$

This simplification is a way of qualitatively taking into account the physical origins of the evolution of the relative permittivity of the material. More accurate calculations would take into account the mutual influence of the permanent dipoles, considering both intramolecular and intermolecular forces, and leading to the complex calculation of the local field (through an improved version of the Clausius–Mosotti relation) [26].

Below T_g: the molecular mobility is negligible. The dipoles being frozen, their molecular polarizability α remains relatively constant, and $d\alpha/\alpha/dT$ is negligible. $d\varepsilon'/\varepsilon'/dT$ therefore mainly accounts for the evolution of effectively probed dipole density N which decreases linearly with the volume thermal expansion. Furthermore, the isotropic nature of the material leads to the simple relation in the following equation:

$$\frac{d\varepsilon'}{\varepsilon'} \approx \frac{dN}{N} = -\frac{d\text{Volume}}{\text{Volume}} \Rightarrow \frac{\frac{d\varepsilon'}{\varepsilon'}}{dT} \approx -\frac{\frac{d\text{Volume}}{\text{Volume}}}{dT} \approx -3\alpha_l \qquad (12)$$

Equation (10) can therefore be simplified with equation (12), leading to the following equation (13).

$$\frac{dV/V}{dT} \approx 4\alpha_l \approx 280.10^{-6} \text{ K}^{-1} \qquad (13)$$

The value obtained through this rather simplistic calculation and the experimental slope (425.10^{-6} K^{-1}) are in the same order of magnitude.

Above T_g: the molecular mobility is obviously not negligible. Therefore, $d\varepsilon'/\varepsilon'/dT$ must account for both the reduction of effectively probed dipole density N and the decrease of molecular polarizability α due to molecular mobility. Low frequency (10^{-2} Hz) DDS measurements (figure 8) evidenced that ε' decreases as the temperature increases. In this experimental setup, as opposed to SPD, the sample is being constrained between metallic electrodes. In other words, the sample volume remains approximately constant and the decrease of relative permittivity primarily accounts for a decreasing molecular polarizability. This is confirmed by the fact that $\varepsilon' \approx 3.2$ remains constant below T_g. Therefore, dN/N
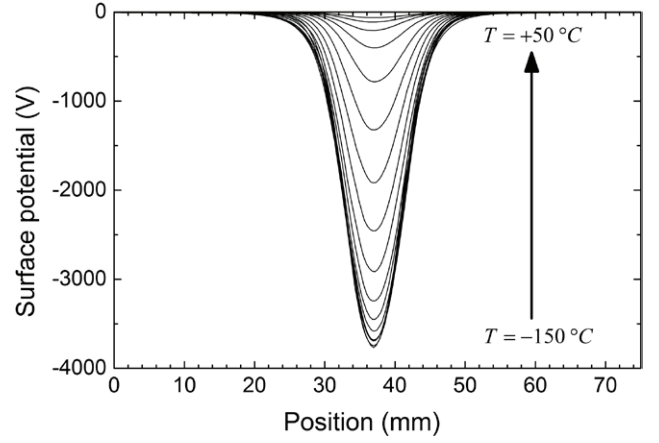
is negligible in the case of DDS measurements but must be taken into account in the case of SPD measurements. This is achieved by measuring the decreasing slope in figure 8 and adding it to equation (13).

$$\frac{dV/V}{dT} \approx -\frac{\frac{d\alpha}{\alpha}}{dT} + 4\alpha_l \approx 2300.10^{-6} \text{ K}^{-1} \qquad (14)$$

Again, in spite of the simplistic approach adopted, experimental (2510.10^{-6} K^{-1}) and calculated slopes are in good agreement above T_g. This shows that contrary to what we initially thought, linear thermal expansion is far from being the only cause of the surprising increase of surface potential with temperature. Indeed, the thickness evolution with temperature influences the capacitance of the sample, its 3D-thermal expansion modifies the probed dipole density (in TSSPD experiments), and molecular mobility dramatically impacts the molecular polarizability above T_g.

3.5. Region II: thermally activated charge transport

The second phenomenon observed in figure 4 consisted in a temperature initiated ($T \approx -50$ °C) current flow through the sample resulting in a quasi-total discharge of the sample as room temperature was reached.

In order to assess the influence of surface conductivity on this current flow, a slight variation of the SPD experiment was performed. By means of a diaphragm of diameter 1.5 mm, the irradiated area of a 75×75 mm^2 sample was reduced to a disc of 30 mm diameter. Charging was therefore performed in the center of the sample at $T = -150$ °C. Then, successive isothermal scans over the length of the sample (figure 9) showed no evidence of lateral diffusion of the deposited charges as temperature was increased, therefore confirming the anticipated [27] negligibility of surface conduction processes in high vacuum.

This volume current flow is difficult to analyze from the TSSPD curve in figure 4 due to the interlinked influence of time and temperature on the potential decay. DDS measurements allow the evaluation of electrical conductivity thanks to
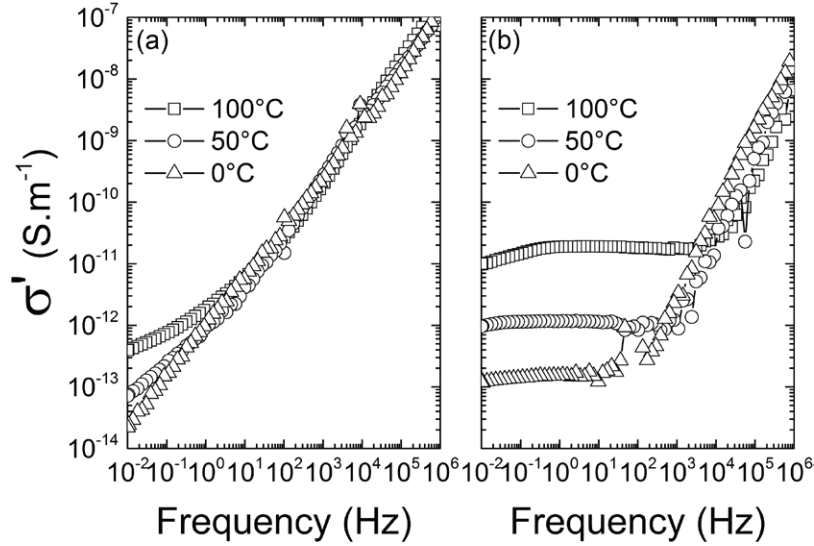
Figure 10. DDS measurements of the real conductivity versus frequency for (*a*) a filled sample and (*b*) a neat sample.
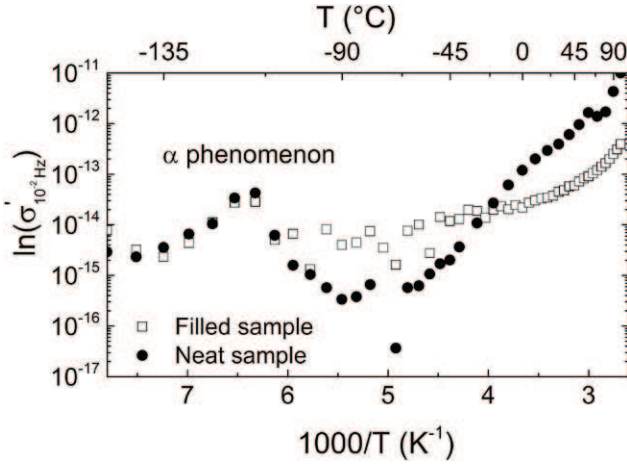

Figure 11. DDS measurements of low frequency conductivity versus temperature for filled and neat samples.

Figure 12. Isothermal surface potential decay curves: −57, −51, −46, −41, −31, −20, −11 and 0 °C.

equation (3). Further development of this equation leads to the following expression:

$$\sigma'(\omega) = \sigma_{DC} + i\omega\varepsilon_0\varepsilon''_{\text{dipolar}} \tag{15}$$

The real part of complex conductivity accounts for classical conductivity (i.e. frequency independent charge transport) and a variety of frequency dependent dielectric phenomena, dipolar for the most part, summed up in the loss term $\varepsilon''_{\text{dipolar}}$.

Jonscher [28] formulated, for disordered systems, a famous empirical power law called 'universal' further to a review of abundant experimental data, linking the real part of the complex conductivity to frequency as follows:

$$\sigma'(\omega) = \sigma_{DC} + A\omega^n \qquad 0 < n \leq 1 \tag{16}$$

where A is a constant, and n the exponent of the power law.

The relation in equation (16) does not fully describe the frequency behavior of $\sigma'(\omega)$. The universality as Jonscher defined it resides in the power law describing the ac component of conductivity. In some cases, however, a low-frequency dc (or quasi-dc, called low frequency dispersion)
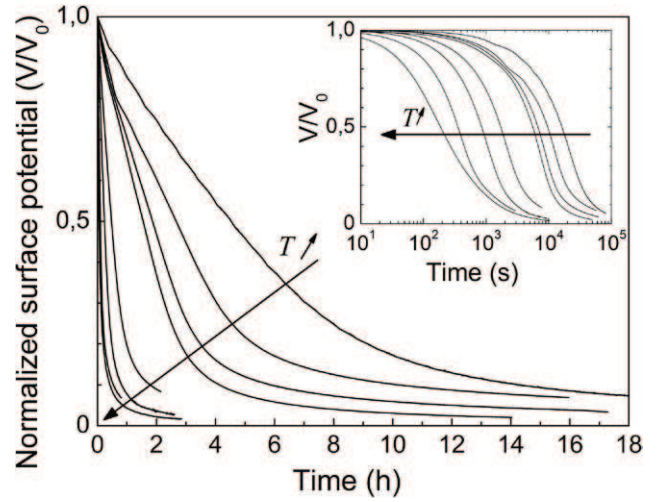
plateau is observed, along with a transition to the dispersive high frequency region at a critical frequency ω_c. The individual treatment of broad frequency regions is named fractional power law.

In figure 10(*a*) are reported three σ' versus frequency curves extracted from isothermal DDS scans performed on a *filled* sample. Although Jonscher's law predictably applies to these results, with $n \approx 1$ at sufficiently high frequencies, no σ_{DC} term can be extracted from any of the three curves. At 0 °C, there is strictly no frequency independent (no dc plateau) contribution superimposed to the ac power law, resulting in a linear dependence of σ' on frequency in the whole frequency range. As temperature increases, a dc contribution gradually increases in the low frequency region, resulting in the progressive bending of the ac straight line. Still, no dc plateau is observed, even at high temperature (+100°C).

DDS measurements were also performed on a neat sample (the fillers of which had been almost entirely removed) and three of them are reported in figure 10(*b*) in the same way as
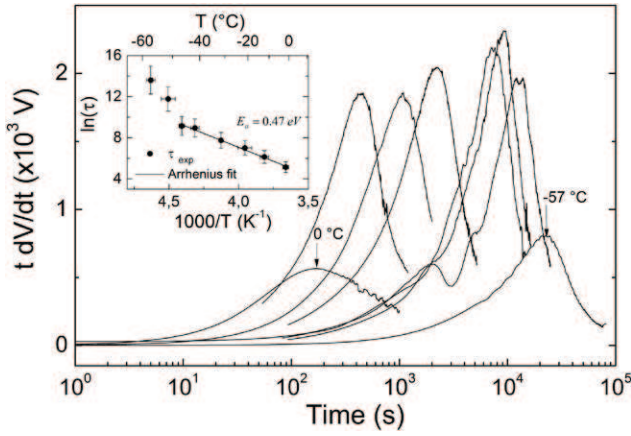
Figure 13. tdV/dt analytical transformations of isothermal surface potential decay curves in figure 12.

figure 10(*a*). The major influence of the silicate and iron oxide fillers on the low frequency electrical behavior of this material becomes evident in the comparison between figures 10(*a*) and (*b*). Indeed, in the absence of fillers, a clear dc contribution—in the form of a plateau—arises at low frequency as the temperature increases. Moreover, the critical (or crossover) frequency ω_c has approximately the same temperature dependence as σ_{DC} [29].

The low frequency (10^{-2} Hz) isothermal DDS conductivities were extracted from *filled* and *neat* isothermal frequency curves such as figure 10; they are represented in an Arrhenius plot in figure 11. In the low temperature range, both curves exhibit the dielectric manifestation of glass transition. The associated peak is the same that appeared in the 3D loss spectrum (figure 2), except that it has been analytically calculated from equation (3).

Bearing in mind the discrepancy between the low frequency electrical behaviors of *filled* and *neat* materials (figure 10), it comes as no surprise that the thermal activation of conductivity at higher temperature is also impacted by the presence of the fillers. Actually, while no obvious thermally activated model can be applied to the filled curve, the neat one displays an Arrhenius behavior from approximately −60 °C and up to 100 °C. The activation energy of this thermally assisted hopping mechanism was found to be 0.39 eV, traducing an electronic charge transport [7, 30].

Isothermal SPD measurements were performed on a filled sample and are reported in figure 12. The temperature of these experiments was limited in the upper range by the inability of the sample to hold a surface charge (too conductive) and in the lower range by too long experimental times (sample not conductive enough to observe a full discharge without eventually running out of liquid nitrogen). The initial surface potential was in most cases set to be close to −4 kV except for the two less charged extreme temperatures.

If the sample was an ideal parallel-plate capacitor (of capacity C and relative permittivity ε') discharging in an ideal resistor (of resistance R and resistivity ρ), its potential decay curve would be perfectly described by a simple exponential function, the time constant of which would be described by the following expression:

$$\tau = RC = \rho \varepsilon_0 \varepsilon' \tag{17}$$

Where ε_0 is the vacuum permittivity.

While the experimental potential curves in figure 12 cannot be fitted by simple exponential functions, a time constant does exist for each isothermal decay, as it can be observed more clearly in the inset plot versus log (t). One efficient way to determine these time constants from the stretched exponential functions is the $t dV/dt$ versus log (t) representation, initially developed by Watson [31] and later successfully applied to corona-charged polypropylene potential decay curves [32]. In a $t dV/dt$ versus log (t) plot, this transformation turns a simple exponential function into a peak centered in the exponential time constant, and its amplitude is proportional to the initial value of the function (initial potential in the case at stake here).

In figure 13 are reported the $t dV/dt$ curves associated with the experimental potential decay experiments in figure 12. This analytical transformation produces well defined peaks from which experimental characteristic times $\tau(T)$ can be extracted with ease. The observed discrepancy in amplitude on the two extreme peaks is explained by their lower initial surface potential.

The experimental characteristic times are reported in an Arrhenius plot in the inset graph of figure 13. Above $T \approx -50$ °C, they are well described by an Arrhenius law with an activation energy of 0.47 eV, which is in the same order of magnitude than that of the neat material obtained in DDS. Below −50 °C, there is a deviation from the previous Arrhenius behavior. In the thermally-stimulated SPD experiment (figure 4), −50 °C is the approximate temperature above which the potential starts decaying rapidly until complete discharge. The presence of the silica and iron oxide fillers could explain the deviation at −50 °C observed in SPD, and the non-Arrhenius behavior of the low-frequency conductivity measured in DDS. Moreover, no deviation was observed with the neat sample in DDS.

Provided that the theoretical equation (17) can be translated to the experimental world (that has been done before [33]), the association of the $t dV/dt$ transformation (with the determination of the time constant $\tau_{SPD}(T)$) and low-frequency DDS permittivity measurements ($\varepsilon'_{10^{-2} \text{ Hz}}(T)$) allows approximating the material's dc conductivity:

$$\sigma(T) = \frac{1}{\rho(T)} \approx \varepsilon_0 \frac{\varepsilon'_{10^{-2} \text{ Hz}}(T)}{\tau_{SPD}(T)} \tag{18}$$

For instance, this estimated conductivity is ~ 2 10^{-13} S.m^{-1} at 0 °C and drops down to ~ 3 10^{-15} S.m^{-1} at −46 °C.

However, the nature of the influence of the fillers on the low frequency electrical behavior is complicated to determine, as it strongly interferes with the charge transport phenomenon. The most straightforward explanation would reside in interfacial polarization (Maxwell–Wagner–Sillars) involving macrodipoles at the fillers/matrix interface. This

hypothesis would account for the detectable, yet too mixed in the thermally activated charge transport to be fitted, peak in figure 2, in the high temperature range. There is ongoing work on this subject, especially via SPD experiments performed on neat samples.

4. Conclusion

The electrical behavior of a commercial silicone elastomer was studied by means of TSSPD, which is a new thermally stimulated dc technique, and DDS, an isothermal ac technique. The dielectric manifestation of the glass transition, around $-116\,°C$, was observed with both of these techniques.

In the low temperature range, a potential drop, induced by dipole orientation, occurs as the glass transition temperature is reached during a TSSPD experiment. Superimposed to it, a linear variation of the surface potential with temperature was evidenced and correlated with the linear thermal expansion of the sample thickness, a dielectric permittivity decrease due to molecular mobility, and a reduction of the probed dipole density via 3D thermal expansion. TSSPD proved to be very suitable for the observation of a dipolar relaxation phenomenon, thus exceeding the traditional fields of this technique, generally focused on charge injection and transport. It also proved to be complementary to the usual experimental tools used in molecular mobility studies that are DDS and TSC analysis.

In the high temperature range, an increasing conductivity due to charge transport was observed with both techniques. It was shown that the silicate and iron(III) oxide fillers play an determining role in the low frequency electrical behavior of this material. DDS indeed evidenced a true dc conductivity component in the case of the *neat* material, not present in the case of the *filled* one. This influence is believed to be of the Maxwell–Wagner–Sillars type, but we lack experimental data to fully characterize it. There is ongoing work on the subject, especially through the use of isothermal SPD and TSC analysis. These techniques measure isothermal dc quantities which provide data that are less complex to interpret in the sense that time and temperature effects are separated, as opposed to TSSPD.

Finally, this study falls within the scope of a more extensive work relating to the effect of radiation ageing on the electrical properties of this space-used silicone elastomer.

References

[1] Biron M 2007 Silicones ou siloxanes *Applications Tech. L'ingénieur Matériaux à Propriétés Mécaniques* n2882

[2] Cohen-Addad J-P 2007 *Polymères: la Matière Plastique* (Paris: Belin)

[3] Bokobza L 2004 Elastomeric composites. I silicone composites *J. Appl. Polym. Sci.* **93** 2095–104

[4] Xu J, Razeeb K M and Roy S 2008 Thermal properties of single walled carbon nanotube-silicone nanocomposites *J. Polym. Sci. B Polym. Phys.* **46** 1845–52

[5] Sau K P, Khastgir D and Chaki T K 1998 Electrical conductivity of carbon black and carbon fibre filled silicone rubber composites *Die Angew. Makromol. Chemie* **258** 11–7

[6] Tuncer E and Gubanski S M 2000 Electrical properties of filled silicone rubber *J. Phys.: Condens. Matter* **12** 1873

[7] Nguyen D H, Sylvestre A, Gonon P and Rowe S 2004 Dielectric properties analysis of silicone rubber *Proc. IEEE Int. Conf. on Solid Dielectrics* vol 1 pp 103–6

[8] Molinié P and Alvarez D 2006 Etude de l'injection de charge sur des plaques d'élastomère silicone par mesures du potentiel de surface *Rev. Int. génie électrique* **9** 389–404

[9] Johansson C and Robertsson M 2007 Broadband dielectric characterization of a silicone elastomer *J. Electron. Mater.* **36** 1206–10

[10] Baker D N 2000 The occurrence of operational anomalies in spacecraft and their relationship to space weather *IEEE Trans. Plasma Sci.* **28** 2007–16

[11] Frederickson A R and Dennison J R 2003 Measurement of conductivity and charge storage in insulators related to spacecraft charging *IEEE Trans. Nucl. Sci.* **50** 2284–91

[12] Paulmier T, Dirassen D and Payan D 2012 Charging behavior of space-used adhesives at low temperature in geostationary orbit *J. Spacecr. Rockets* **49** 115–9

[13] Berlepsch H V 1985 Interpretation of surface potential kinetics in HDPE by a trapping model *J. Phys. D: Appl. Phys.* **18** 1155

[14] Sahli S, Bellel A, Ziari Z, Kahlouche A and Segui Y 2003 Measure and analysis of potential decay in polypropylene films after negative corona charge deposition *J. Electrostat.* **57** 169–81

[15] Xu Z, Zhang L and Chen G 2007 Decay of electric charge on corona charged polyethylene *J. Phys. D: Appl. Phys.* **40** 7085

[16] Molinie P, Goldman M and Gatellet J 1995 Surface potential decay on corona-charged epoxy samples due to polarization processes *J. Phys. D: Appl. Phys.* **28** 1601–10

[17] Kremer F and Schönhals A 2003 *Broadband Dielectric Spectroscopy* (Berlin: Springer)

[18] Lacabanne C and Chatain D 1973 Depolarization thermocurrents in amorphous polymers *J. Polym. Sci. A-2 Polym. Phys.* **11** 2315–28

[19] Tomaszewicz W 2001 Surface-potential decay of disordered solids *J. Electrostat.* **51–52** 340–4

[20] Mizutani T, Oomura T and Ieda M 1981 Surface potential decay in polyethylene *Japan. J. Appl. Phys.* **20** 855

[21] Lötters J C, Olthuis W, Veltink P H and Bergveld P 1997 The mechanical properties of the rubber elastic polymer polydimethylsiloxane for sensor applications *J. Micromech. Microeng.* **7** 145

[22] Fragiadakis D, Pissis P and Bokobza L 2005 Glass transition and molecular dynamics in poly(dimethylsiloxane)/silica nanocomposites *Polymer (Guildf).* **46** 6001–8

[23] Brandrup J, Immergut E H, Grulke E A, Abe A and Bloch D R 1999 *Polymer Handbook* vol **89** (New York: Wiley)

[24] Havriliak S and Negami S 1966 A complex plane analysis of α-dispersions in some polymer systems *J. Polym. Sci. C Polym. Symp.* **14** 99–117

[25] Smyth C P 1955 *Dielectric Behavior and Structure* (New York: McGraw-Hill)

[26] Blythe A R and Bloor D 2005 *Electrical Properties of Polymers* (Cambridge: Cambridge University)

[27] Coelho R 1985 The electrostatic characterization of insulating materials *J. Electrostat.* **17** 13–27

[28] Jonscher A K 1999 Dielectric relaxation in solids *J. Phys. D: Appl. Phys.* **32** R57

[29] Dyre J C and Schrøder T B 2000 Universality of ac conduction in disordered solids *Rev. Mod. Phys.* **72** 873–92

[30] Wang Y 2008 Ionic and electronic transport in conducting polymer systems *PhD Thesis* University of Oregon

[31] Watson P K 1995 The transport and trapping of electrons in polymers *IEEE Trans. Dielectr. Electr. Insul.* **2** 915–24

[32] Llovera P and Molinie P 2004 New methodology for surface potential decay measurements: application to study charge injection dynamics on polypropylene films *IEEE Trans. Dielectr. Electr. Insul.* **11** 1049–56

[33] Haenen H T M 1975 The characteristic decay with time of surface charges on dielectrics *J. Electrostat.* **1** 173–85